Catal Lett (2009) 127:204–212
DOI 10.1007/s10562-008-9671-6

Novel Utilization of Zeolited Fly Ash Hosting Cobalt Nanoparticles as a Catalyst Applied to the Fischer–Tropsch Synthesis

F. Fotovat · M. Kazemeini · H. Kazemian

Received: 30 July 2008 / Accepted: 13 September 2008 / Published online: 7 October 2008

Abstract In order to produce an inexpensive catalyst for the Fischer–Tropsch synthesis (FTS), zeolitized high silicon fly ash utilized as a catalytic support for cobalt nanoparticles. The ability of this new support in proper hosting of nanoparticles studied through various characterization methods such as X-ray diffraction, nitrogen sorption, transmission electron microscopy, energy-dispersive spectroscopic and temperature-programmed reduction. In addition, the catalytic properties for the FTS evaluated at 523 K and 20 MPa. The obtained results show remarkable influence of utilized support specifications upon the formation and catalytic behavior of cobalt nanoparticles in the FTS.

Keywords Zeolite · Fly ash · Fischer–Tropsch synthesis · Nanoparticles · Porous structure

1 Introduction

The importance of the Fischer–Tropsch synthesis (FTS) process (synthesis of hydrocarbons from CO and H_2) as the main step of gas to liquid (GTL) technology is increasing due to various factors such as the vast reserves of natural gas against the decreasing volume of crude oil reserves throughout the world, and the rising value and applications of middle distillates. Furthermore, the growing demands for cleaner fuels, the stiffer standards for fuels and pertinent contamination, the free-sulfur property of synthetic distillates, in addition to the increasing price of crude oil and the growing efficiency of GTL process has renewed the interest of using natural gas as a potential source of hydrocarbons [1]. In other words, the Fischer–Tropsch process is considered as the most significant replacement for petroleum to produce clean hydrocarbon fuels with high cetane number and other value-added products [2–4].

The role of the catalyst used in the FTS is completely pivotal to achieve the most desirable product such as long-chain n-paraffins. It is shown that besides the kind and size of the active metal phase (i.e., Fe, Co, Ru), the characteristics of the catalysts' supports have direct influence on the products quality and quantity via altering the activity, stability, and product selectivity of the catalyst [5]. Although the circumstance of support effects on the behavior of catalysts is not completely vivid [6], it is reported that the structure and porosity of support affects the distribution and reducibility of the active metal phase particles precipitated on it [7–9]. In recent years, many investigators have been interested in micro- and mesoporous molecular sieves as supports for preparing the FTS catalysts, due to their ability to amend the catalyst activity and selectivity [10–14]. In addition, the narrow and ordered channels of these materials create a proper bed for formation of metal and metal oxide nanoparticles [15, 16]. Natural or synthesized zeolites are a well-known family of these materials, possessing unique properties to be utilized as catalytic supports. Applying different types of zeolites

F. Fotovat · M. Kazemeini (✉)
Department of Chemical and Petroleum Engineering,
Sharif University of Technology, Azadi Ave,
P.O. Box 11365-9465, Tehran, Iran
e-mail: kazemini@sharif.edu

H. Kazemian
R&D Lab. of SPAG Co., Technology Incubator,
Sci and Technol. Park of Tehran University, Tehran, Iran

H. Kazemian
NSTRI, P.O. Box: 11365-3486, Tehran, Iran

for encapsulating nanosized metal particles was suggested some years ago [17–20].

Faujasite zeolites, including X- and Y-type zeolites, have ordered void volumes known as supercages in their unit cell that make them as desirable hosts for the preparation of metal nanoparticles such as Pd, Pt, Rh, Au, Ag and Cu [21–28]. Moreover, exploitation of faujasite zeolites as catalytic supports is very widespread because of their desirable properties such as high thermal stability and mechanical strength.

Notwithstanding the fact that faujasitic zeolites may be found in both natural and synthetic forms, the catalytic applications of the synthetic forms are more prevalent due to their properties, which are more acceptable. However, the costs of producing such zeolite are much higher than that of natural ones. In recent years, various methods have been suggested to generate faujasite in high tonnage from cheap impure raw materials such as kaolin [29–31] or fly ash [32–34]. Utilizing these materials significantly reduces the overall costs of zeolite synthesizing. It is estimated that a utility may convert its own fly ash into zeolite-containing materials for approximately $50–100 per ton [35]. In addition, the cost of such materials synthesized from fly ash zeolite was estimated to be almost one-fifth of the commercial 13X zeolite available in the market [36]. To these authors knowledge, there is still no report on exploitation of zeolites produced from impure materials in catalytic fields.

In this paper, studies on deposition of cobalt nanoparticles into the LTA (Linde type A) and FAU (Faujasite) zeolites synthesized from high silicon fly ash (HSFA) are reported. Furthermore, catalytic behaviors of these prepared cobalt nanoparticles in the Fischer–Tropsch synthesis are investigated.

2 Experimental

2.1 Preparation of Catalysts

The zeolitic supports with Si/Al ratios varying approximately from 1.2 to 1.6 were synthesized from HSFA according to the procedure described in previous work of these authors [37]. In addition, one faujasitic sample was synthesized from pure chemical materials according to the Ref. [38]. Beside all of these samples, a commercial faujasite sample was obtained from Aldrich Chemical Company as the standard support. In order to deposit cobalt particles on supports via ion-exchange, 1 g of each zeolitic sample was added to 0.1 molar aqueous solution (50 mL) of cobalt nitrate ($Co(NO_3)_2 \cdot 6H_2O$) and this mixture was shaken periodically for 40 h at 300 rpm and room temperature. In a similar way to the work of Tang et al. [39] after filtration, washing carefully with deionised water, and drying at 333 K for 10 h, each cobalt-exchanged zeolite was chemically treated with a 100 mL of 0.1 molar NaOH solution under stirring in order to precipitate cobalt hydroxide inside zeolite pores and consequently facilitate the reduction process. This step was finalized through vacuum filtration, regulating the pH around 7.0, and drying at 393 K for 3 h. The powdery product was calcined at 673 K for 6 h. The applied ramp rate of heating/cooling before/after calcination was 1 K/min.

2.2 Characterization Techniques

The silicon, aluminum, and cobalt content of each sample were determined by Inductively Coupled Plasma Atomic Emission (ICP-AE) spectroscopy using a Perkin Elmer Elan Optima 3000DV after ion-exchange step. X-ray diffraction (XRD) patterns were obtained at room temperature using XRD spectrometry (Philips Analytical, Cu Ka radiation).

Textural properties of supports and Co-containing catalysts were obtained from the nitrogen sorption experiments carried out at 77 K using BELSORP-MINI II (Apollo Instruments Co., Japan). Prior to determination of the adsorption isotherm, the sample was out gassed. A heating mantle then applied to the sample tube and the contents heated under vacuum to 423 K for 12 h. The sample was then immersed in liquid nitrogen at 77 K before the sorption measurements were taken. BET (Brunauer–Emmett–Teller) equation was used to determine the specific surface area and pore volume of selected samples. The pore-size distributions were derived from the nitrogen adsorption isotherms at 87 K using the BJH (Barrett–Joyner–Halenda) method.

Bright and dark-field transmission electron microscopy (BF, DF-TEM) with X-ray energy-dispersive spectroscopic analysis (EDS) was carried out by Hitachi 800MT microscope operated at an accelerating voltage of 200 kV to clear cobalt oxide particle-size distribution. For the TEM measurements, the solids were dispersed in acetone and dropped on a copper microgrid covered by a holey carbon film. The obtained images were analyzed through image processing technique.

The reduction behaviors of encapsulated cobalt oxide particles studied by CHEMBET-3000 Quantachrome using temperature-programmed reduction (TPR) method on a flow system equipped with a thermal conductivity detector. About 100 mg of calcined catalyst was placed into a quartz reactor and reduced in situ at 1273 K for 10 h at a heating rate of 1 K/min by flowing 10 cm^3/min of a mixture of 10 vol% H_2 in Ar and the H_2 consumption registered.

2.3 Catalytic Experiments

The Fischer–Tropsch synthesis reaction was performed in a standard laboratory fixed bed stainless-steel microreactor (d_i = 10 mm, l = 40 cm) presented schematically in Fig. 1. Three mass flow controllers (Brooks, Model 5850E) equipped with a four-channel control panel (Brooks 0154) were used to adjust automatically the flow rate of the inlet gases (CO, H_2, and N_2 with purity of 99.999%).

The mixed gases passed into the reactor tube, which was placed inside a tubular furnace (Atbin, Model ATU 150-15) controlled by a digital programmable controller. The 60–120 meshed catalyst (1.0 g) was held in the middle of the reactor tube with 70 cm length using quartz wool. Prior to the catalytic experiments the catalysts were reduced in situ at atmospheric pressure by increasing the temperature at a heating rate of 1 K/min up to 673 K and maintained at this temperature for 5 h while passing a flow of pure hydrogen (30 cm^3/min) through the reactor. After the reduction step the temperature was decreased to 373 K under the flow of H_2 and then the reactant gas mixture was introduced at a total flow rate of 250 cm^3/min (H_2/CO = 2), and the reactor pressure slowly increased up to 20 bar. Then, the temperature in the catalyst bed was increased to 523 K at a controlled heating rate of 5 K/min. Once achieving this temperature, the reaction was led to proceed during a period of 20 h to ensure stabilization of the catalyst activity. Reactant and product steams were analyzed on line using a gas chromatograph (Varian, Model 3400 series) equipped with a 10-port sampling valve (Supelco company, USA, Visi Model), a sample loop and a thermal conductivity detector. The contents of sample loop were injected automatically into a packed column (Haye-sep DB, Alltech Company, USA, 1/800 o.d., 10 m long, and particle mesh 100/120). Helium was employed as a carrier gas for optimum sensitivity. GC controlling and collection of all chromatograms was done via an IF-2000 single channel data interface (TG Co., Teheran, Iran). The CO conversion (%) and the reaction selectivity (%) towards one product such as j were calculated according to the below relations, respectively.

$$\text{CO Conversion } (\%) = \frac{\text{moles}CO_{in} - \text{moles}CO_{out}}{\text{moles } CO_{in}} \times 100$$

$$\text{Selectivity of product j } (\%) = \frac{\text{moles of j produced}}{\text{moles } CO_{in} \text{ - moles } CO_{out}} \times 100$$

3 Results and Discussion

Molar Si/Al ratio of all catalytic supports (denoted as Z-1 to Z-5) and the cobalt contents of their ion-exchanged forms (denoted as Co/Z-1 to Co/Z-5) determined through ICP-AE spectroscopy are shown in Table 1. Considering the fact that performing preparation steps after the ion exchange has no influence on the cobalt content of final catalytic samples [40], one may assume cobalt content values presented in this table as those of final catalysts. As expected, in a specific type of zeolites such as faujasitic

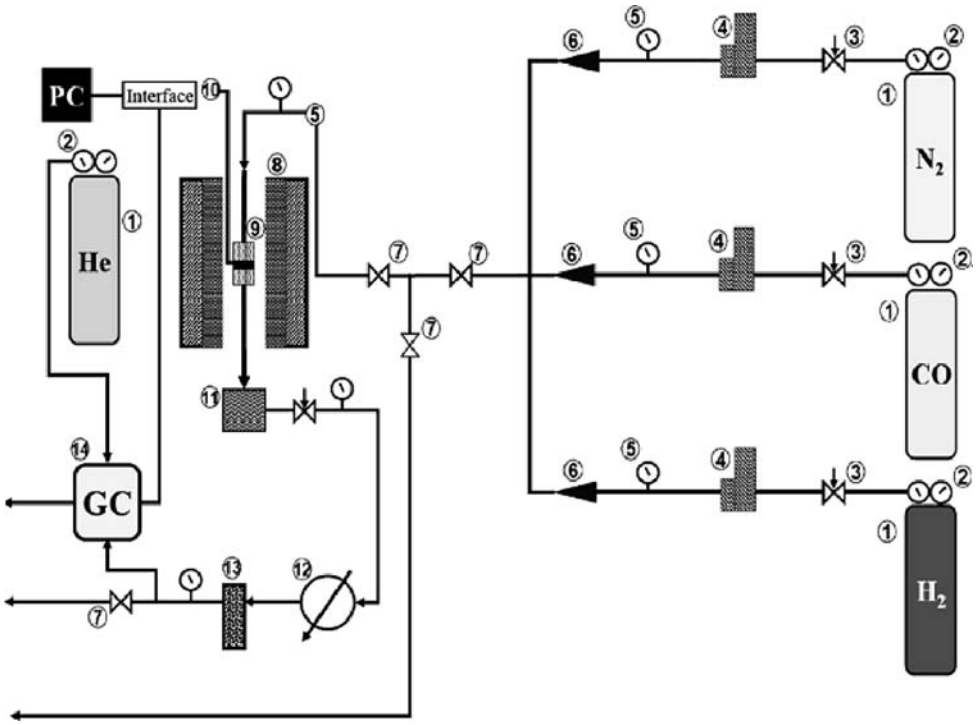

Fig. 1 Schematic representation of the reactor used. (1) Gas cylinders, (2) pressure regulators, (3) needle valves, (4) mass flow controllers (MFC), (5) monometers, (6) non-returns valves, (7) ball valves, (8) tubular furnace, (9) reactor, (10) catalyst bed, (11) trap, (12) condenser, (13) silica gel column and (14) gas chromatograph (GC)

Table 1 Molar Si/Al ratio and Cobalt content of different Co catalysts used in FT reaction

Catalyst	Molar Si/Al ratio of related support	Co (wt%)	Remarks about the related support
Co/Z-1	1.19	9.5	Synthesized from HSFA
Co/Z-2	1.4	12.57	Synthesized from HSFA
Co/Z-3	1.53	10.98	Synthesized from HSFA
Co/Z-4	1.83	11.97	Synthesized from pure materials
Co/Z-5	2.29	9.37	Commercial faujasite

zeolites the higher the molar Si/Al ratio of a support, the lower cobalt content resulted. It should be noted that this rule is limited to only one type of zeolites and as a result, the Si/Al value of sample Co/Z-1 belonging to LTA family should not be compared with those of other samples. This behavior is attributed to the less cation exchange capability (CEC) of zeolites with more Si/Al ratio. Despite the negative effects of impurities on the CEC of samples supported by synthetic zeolites, their comparably high cobalt content is a promising point for their good catalytic performance. It is also noteworthy that some of these samples such as Co/Z-2 can have higher cobalt content than Co/Z-4 the support for which was synthesized from chemically pure materials. Further, the cobalt content of all of the synthesized samples is greater than that of some new micro- and mesoporous materials such as MCM-22 [41].

Figure 2 shows the XRD patterns of the calcined samples. All of the main visible peaks in these patterns are ascribed to LTA and faujasitic (NaX or NaY) zeolites. This issue indicates the stability of the supports synthesized from HSFA after various thermal and chemical treatments during catalyst preparation process. However, as displayed in Fig. 2 different supports have different purities and as expected catalysts with supports synthesized from HSFA such as Co/Z-2 have less intense peaks in their XRD patterns in comparison with samples with standard supports such as Co/Z-4. Furthermore, the absence of any detectable peak related to cobalt oxides (CoO or Co_3O_4) in the XRD pattern of catalyst Co/Z-2 reveals that the size of crystalline cobalt oxide particles in this sample should not exceed a few nanometers comparable with the size of faujasite supercages [39].

The structural properties of some of the zeolitic supports and corresponding catalysts (including Co/Z-2 as a sample with a base synthesized from HSFA and Co/Z-4 and Co/Z-5 as samples having standard bases) derived from the N_2 adsorption isotherms are summarized in Table 2. The uniformity of the pores before and after cobalt deposition is understood through similar inflection trends of N_2 adsorption isotherms of Z-2 and Co/Z-2 (Fig. 3a). These isotherms, which belong to the type-I of adsorption models, typify the prevalent microporous structure of the utilized

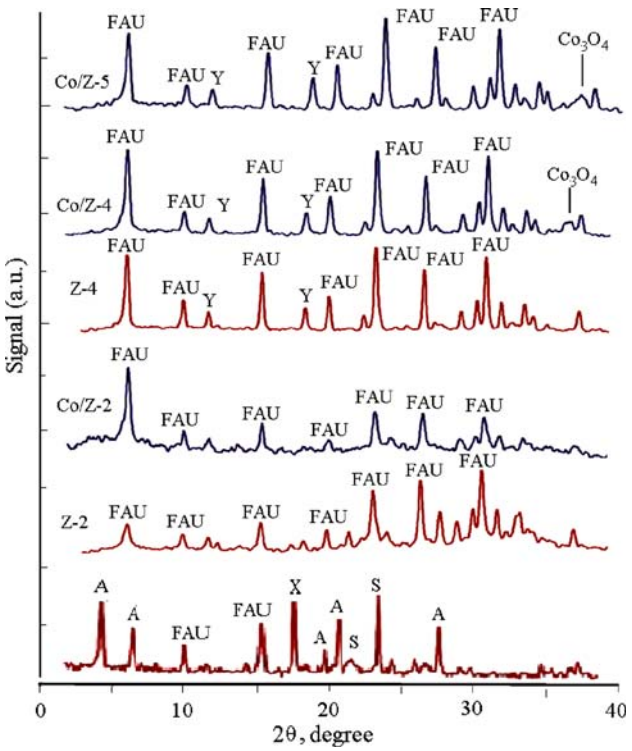

Fig. 2 Powder XRD patterns of Z-1, Z-2, and Z-4 faujasitic supports and Co/Z-2, Co/Z-4 and Co/Z-5 catalysts. Symbols A, X, Y, FAU, and S denote the peaks of A, X, and Y zeolites, faujasite, and sodalite, respectively

Table 2 Textural properties of faujasitic supports and relevant Co-containing catalysts determined by nitrogen adsorption

Support/Catalyst	S_{BET} (m^2/g)	Total pore volume (cm^3/g)	Mean pore diameter (nm)
Z-2	434.76	0.362	3.33
Co/Z-2	406.66	0.401	3.95
Z-4	714.24	0.380	2.13
Co/Z-4	619.26	0.358	2.31
Z-5	720.11	0.306	1.70
Co/Z-5	701.5	0.343	1.95

supports [40]. In addition, the similarity of the pore-size distribution for these samples determined by nitrogen adsorption at 87 K using the BJH method (see Fig. 3b) shows that despite the existence of cobalt oxide particles, the Co-containing synthetic faujasites may preserve their porous structure as indicated by XRD results (Fig. 2). A discrepancy about the right value of mean pore diameter of catalyst Co/Z-2 and support Z-2 may be perceived by comparing their mean pore diameter values reported in Table 2 with the plots of Fig. 3b presenting their pore-size distribution. This superficial discrepancy originates from presenting the distribution of all pores (from micro to macropores) in these plots and not focusing on the

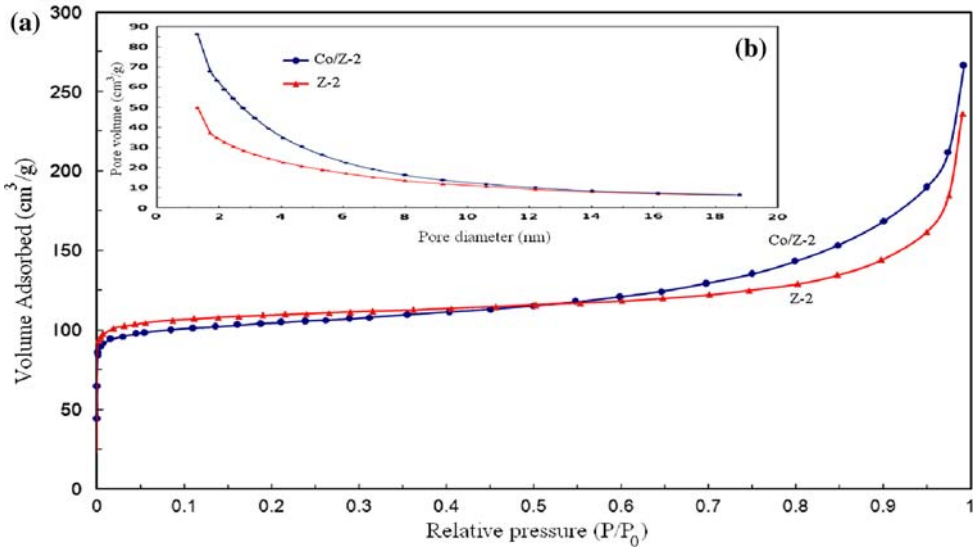

Fig. 3 (**a**) Nitrogen adsorption isotherms obtained at 77 K for: Z-2 and Co/Z-2. (**b**) Pore-size distributions of these two samples obtained from nitrogen adsorption at 87 K using the BJH method

distribution of micropores only. In other words, since the value of mean pore diameter is about the size of micro or mesopores, plots presenting micro/mesopores size distribution may result in mean pore diameters coinciding to the values reported in Table 2.

It is proven that the enlargement of the mean pore diameters of cobalt-exchanged faujasites in comparison with their primary state is an evidence for deposition and modest growth of cobalt particles inside micro or mesopores [41]. As a result, the size of cobalt oxide particles as the precursors of metal active phase may be controlled in this way. Since sample Co/Z-2 has the wider mean pore diameter than those of two other samples given in Table 2, the encapsulation of cobalt particles inside of its pores is more probable and consequently the pattern of cobalt oxides deposition into it is remarkably homogenous. It should be noted that pore volumes might increase versus the decrease of the specific surface area after incorporation of Co, as occurred for samples Co/Z-2 and Co/Z-5. Assuming cylindrical pore geometry, changes in dimensions of pores under specific conditions after deposition of Co into pores might be a possible explanation for observing such behavior. In other words, after deposition of cobalt particles, pore diameters might increase a little due to pore wall expansion caused by the moderate growth of Co particles inside the pores exerting pressure outward. In addition, effective length of pores (facing the adsorbate in porosimetery) may decrease due to the partial blockage of pores and/or collapse of porous space due to Co particles deposition. Consequently, the aforementioned variations in the specific surface area versus the total pore volume of sample may take place. It is noteworthy that in this research, related physisorption experiments performed in triplicates and the results reported were completely reproducible for all three runs.

The TEM micrographs and chemical analyses of samples are shown in Fig. 4. The cobalt oxide nanoparticles of sample Co-Z-2 are evident as shiny spots in the related dark-field image (Fig. 4a). One of the several EDS spectra obtained from this sample is shown in Fig. 4b. The similarity of the overall format of these spectra reveals uniform distributions of cobalt in this sample. The more exact position of cobalt particles in relation to the pores of catalyst Co/Z-5 may be obtained from Fig. 4c. In this figure, two different types of dark contrast formed by cobalt particles are perceivable. Since the results of EDS analyses of the darker regions show very intense peaks of Co in comparison with the other peaks such as Si and Al, it is reasonable to attribute darkness to existence of cobalt particles or agglomerates.

In locations in which the dissimilarities between supports and cobalt particles are imperceptible (marked with black arrows), the existence of cobalt oxide particles inside the pores is most likely. On the other hand, the higher contrast of zones marked with white arrows is attributed to the cobalt particles on the external surface of pores [15]. As shown in Fig.2, the appearance of a weak peak at $2\theta = 36.9°$ in the related XRD pattern is another sign for the presence of such particles. The cobalt oxide particle-size distribution of about 80 particles in sample Co/Z-2 is presented in Fig. 5. The size of cobalt particles are distributed in a narrow range, varying between 0.7 and 2.5 nm, with a maximum at 1.3–1.5 nm.

In addition to the aforementioned observations, the similarity between size of particles and support mean pore diameter is another issue denoting the precipitation of nanoparticles inside the supercages and the mesopores of zeolites.

The reduction behavior of the supported cobalt oxide particles in samples Co/Z-2 and Co/Z-5 has been studied

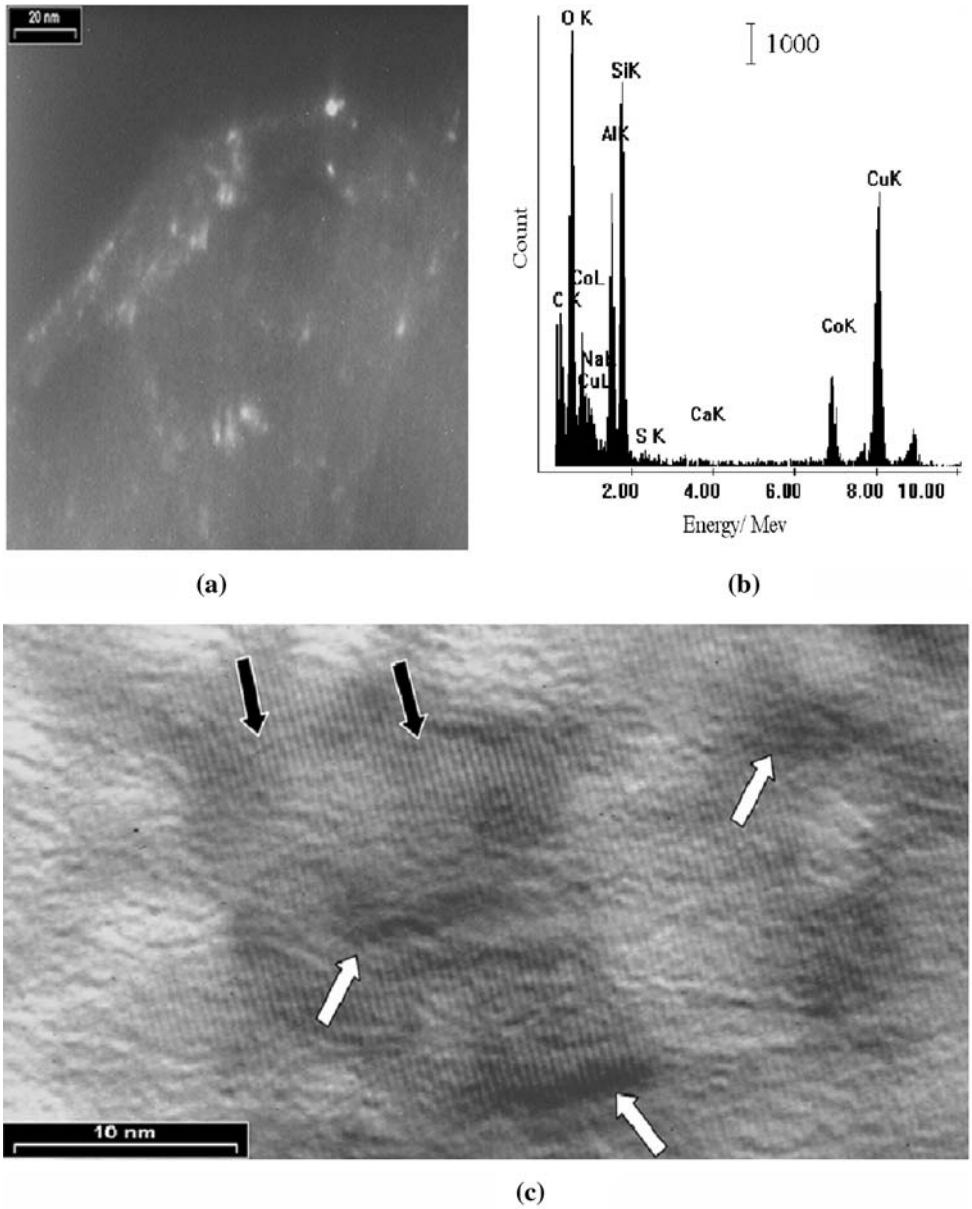

Fig. 4 TEM images and analyses (**a**) dark-field image of sample Co/Z-2, (**b**) EDS spectra of this sample and (**c**) high resolution image of sample Co/Z-5

by temperature-programmed reduction (TPR). The corresponding reduction curves are shown in Fig. 6. The TPR profiles have been normalized per weight of accompanying cobalt of each catalyst. Two broad reduction peaks are observable in TPR diagram of sample Co/Z-2 at temperature ranges of 500–700 and 800–1,150 K. The broadness of these peaks has been assigned to the cobalt species located inside the pores of the zeolite [40]. Considering reduction peaks observed for CoO, Co_3O_4, and the supported cobalt oxides, it seems that the first peak appears due to the reduction of encapsulated cobalt oxide particles most of which are in CoO form [42, 43]. The second peak that occurs at very high temperatures is relevant to the gradual reduction of the highly dispersed Co ions, which are not converted to oxide phase during treatment with NaOH or some of the residual cobalt oxide particles having strong interaction with the faujasite framework [40]. It is seen that, the reducibility of this sample is remarkably different from that of sample Co/Z-2. One possible reason for these variations might be the narrower mean pore diameter of the support that reduces the confining chance of cobalt particles inside the micro or mesopores. In other words, with respect to sample Co/Z-2, due to the narrower mean pore diameter of Co/Z-5 support, the deposition of cobalt particles inside its micro/mesopores is more difficult and consequently the formation of cobalt oxide clusters agglomerated on the surface of pores is more probable. As a result, the two sharp peaks of TPR profile of catalyst Co/Z-5 are attributed to stepwise reduction of relatively large Co_3O_4 particles to Co^0 occurring at moderate temperatures

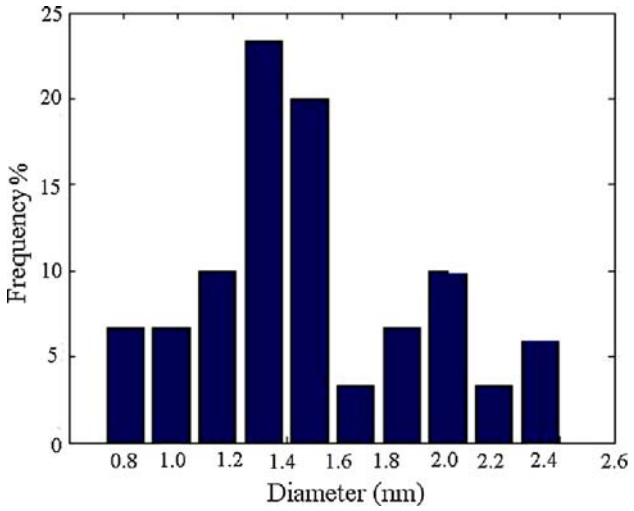

Fig. 5 Cobalt particle-size distribution for sample Co/Z-2 as determined by TEM

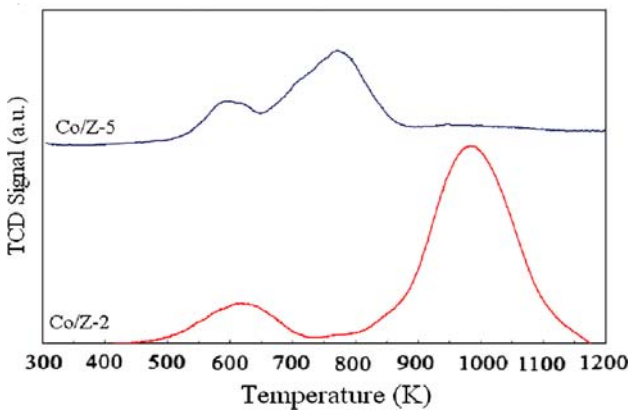

Fig. 6 TPR profiles of samples Co/Z-2 and Co/Z-5

[39]. This seems to be a reasonable conclusion because the smaller size of metallic cobalt particles, the higher temperature needed for reduction [6] as observed for catalyst Co/Z-2 in Fig. 6. Furthermore, the increase in the residence time of the water formed inside the pores (i.e., its slow diffusion rate) during the reduction is yet another reason for the lower reduction degree of small cobalt particles confined in narrow pores [44].

The catalytic activity of the synthesized catalysts was tested in terms of conversion of synthesis gas to light olefins in a fixed-bed reactor under typical hydrocarbon synthesis conditions: 523 K, 20 bar, $H_2/CO = 2$, and gas hourly space velocity (GHSV) of 15 $L_{syngas}/(g_{cat}$ h). The activity and selectivity results for the pseudo-stationary period (10–15 h on stream) are presented in Table 3. As observed, the catalytic behavior of all catalysts supported by zeolites synthesized from HSFA is comparable with those of other synthetic catalysts. Furthermore, from the CO conversion point of view, sample Co/Z-1 is the most

Table 3 Catalytic results for the Fischer–Tropsch synthesis on Co catalysts

Catalyst	CO conv. (%)	Hydrocarbon distribution (%C)		
		C_1	C_2–C_4	C_{5+}
Co/Z-1	53.2	13.8	15.2	53.7
Co/Z-2	36.4	22.4	14.6	48.3
Co/Z-3	45.6	18	29.2	34.1
Co/Z-4	38.2	9.6	20.2	43.7
Co/Z-5	51.2	30.5	28.8	31.6

active catalyst amongst all prepared in this work. Nevertheless, a few shortcomings such as the relatively low CO conversion of sample Co/Z-2 may possibly be attributed to the reduction difficulties and restrictions experienced by this material. It has been well proven that in addition to the extent of cobalt dispersion, the limitations of Co-based FTS catalysts in conversion of CO to hydrocarbons is a proper criterion to determine their reducibility extent [15]. In the case of sample Co/Z-2, due to the high dispersion of cobalt oxide nanoparticles shown previously by TEM results, it is reasonable to deduce that its low activity results from the temperature limit exerted for the reduction step. The relatively high methane selectivity of this sample might be another side effect of this issue, though this value is lower than that of sample Co/Z-5 for which the support is synthesized from commercial faujasite. As observed in Fig. 6, the main reduction peak of sample Co/Z-2 takes place at temperatures more than 800 K, while the maximum boundary of reduction temperature applied in present experiments was set conservatively to 673 K due to possible harmful effects of higher temperatures. In the case of catalyst Co/Z-2, exerting such a thermal limitation leads to leaving a significant amount of unreduced cobalt oxide after reduction causing the conversion of CO to decrease. In comparison with this material, for the case of catalyst Co/Z-5, since the majority of cobalt oxides are reduced under the same thermal applied conditions, the conversion of CO to hydrocarbons is higher despite its lower total cobalt. According to the thermogravimetric analysis (TGA) and scanning calorimetry (SC) curves [37], however the synthesized supports are thermally stable at high temperatures, migration of a large proportion of cobalt particles out of faujasite supercages and pores is more likely at higher reduction temperatures [40]. The results obtained by Tang et al. shows that the formation of longer hydrocarbon chains during the FTS benefits from cobalt particles being located inside faujasite supercages through adjusting the length of hydrocarbon chains properly. The suggested interpretation for such behavior is the re-adsorption of the reaction intermediates increasing the probability of higher hydrocarbons formation as well as provision of a finite

space to restrict the formation of very long chains [39]. In a few words, a compromise between the desirable extent of reduction and the effective dispersion of particles should be considered when such catalysts are being synthesized.

Results of this research are consistent with this observation. A binary comparison between samples Co/Z-2 and Co/Z-4 with Co/Z-3 and Co/Z-5 confirms the inverse relation of CO conversion and C_{5+} selectivity for these samples. Notwithstanding the high CO conversions of Co/Z-3 and Co/Z-5, their C_{5+} selectivities are significantly lower than those of Co/Z-2 and Co/Z-4. On the other hand, samples Co/Z-2 and Co/Z-4 having similarly low CO conversions are more selective towards the formation of C_{5+} than Co/Z-3 and Co/Z-5. This contradictory behavior is related to opposing effects of degree of reducibility and dispersion extent of supported cobalt oxide particles on the catalyst function [45]. Both of these parameters control the density of surface cobalt metal sites that undertake the catalytic role during the reaction [46].

The C_{5+} selectivities of samples Co/Z-1, Co/Z-2, and Co/Z-3, for which their supports correspond to NaA, NaX, and NaY zeolites, respectively, follow a drastically decreasing trend. This trend in present work springs from the purity and crystallinity degree of the zeolites produced from HSFA. In other words, the purer phase of the synthesized zeolitic supports the higher selectivity towards longer produced hydrocarbons is attainable. Furthermore, considering the values presented in Tables 2 and 3, it seems that broadening of the mean pore diameter of the same types of zeolites may help to increase the catalyst selectivity towards heavier hydrocarbons. This observation shows the important effects of a proper catalytic support on achieving the desirable distribution of reaction products that is consistent with the work of Reuel and Bartholomew [47] versus the results obtained by Iglesia [48]. Ultimately, the most successful amongst all samples synthesized in the aforementioned operative conditions in present study is Co/Z-1 having simultaneously high CO conversion and selectivity towards C_{5+}. It appears that the primacy of this sample to others results from the high purity and the completely ordered porous structure of the zeolited HSFA support utilized in it. Hence, highly desirable catalytic results from the same type of synthetic supports with higher purity and crystallinity are foreseeable.

4 Conclusion

In this study, applications of different types of zeolites synthesized from fly ash as inexpensive supports of cobalt-based Fischer–Tropsch catalysts are investigated. Utilizing fly ash in the synthesis of the zeolitic supports resulted in LTA and FAU zeolites with a very high CEC and final cobalt content. The similarity between the XRD results of the bases and the catalytic samples confirmed the stability of these zeolites against the chemical and thermal treatments employed during catalyst preparation. Moreover, BET and TEM results demonstrated well-formed porous structure and deposition of nanosized cobalt particles inside of the micro and mesopores of supports. These obtained results helped to interpret the observed catalytic behaviors of catalysts with different types of supports. In this direction, some properties of support such as its purity, molar Si/Al ratio, and type of the zeolitic support affecting the catalytic performance of the synthetic samples significantly, were identified.

Acknowledgements The authors are expressing their outer most gratitude to Prof. A. A. Mirzaei for his kind assistance and discussion. In addition, they would like to express their thankfulness to the NSTRI, Tehran, Iran for their partial financial support of this project.

References

1. Schulz H (1999) Appl Catal A 186:3
2. Dry ME (2001) J Chem Technol Biotechnol 77:43
3. Gregor JH (1990) Catal Lett 7:317
4. Dry ME (2002) Catal Today 71:227
5. Li H, Li J, Ni H, Song D (2006) Catal Lett 110:71
6. Khodakov AY, Griboval-Constant A, Bechara R, Zholobenko VL (2002) J Catal 206:230
7. Riva R, Miesner H, Vitali R, Del Piero G (2000) Appl Catal A 196:111
8. Jacobs G, Das TK, Zhang Y, Li J, Racoillet G, Davis BH (2002) Appl Catal A 233:263
9. Ernst B, Libs A, Chaumette P, Kiennemann A (1999) Appl Catal A 186:145
10. Ohtsuka Y, Takahashi Y, Noguchi M, Arai T, Takasaki S, Tsubouchi N, Wang Y (2004) Catal Today 89:419
11. Panpranot J, Goodwin JG Jr, Sayari A (2002) Catal Today 77:269
12. Griboval-Constant A, Khodakov AY, Bechara R, Zholobenko VL (2002) Stud Surf Sci Catal 144:609
13. Khodakov AY, Bechara R, Griboval-Constant A (2002) Stud Surf Sci Catal 142:1133
14. Wang Y, Noguchi M, Takahashi Y, Ohtsuka Y (2001) Catal Today 68:3
15. Martínez A, López C, Márquez F, Díaz I (2003) J Catal 220:486
16. Suvato S, Pakkanen TA (2000) J Mol Catal A: Chem 164:273
17. Suzuki M, Tsutsumi K, Takahashi H, Saito Y (1988) Zeol 8:284
18. Suzuki M, Tsutsumi K, Takahashi H, Saito Y (1988) Zeol 8:381
19. Koh DJ, Chung JS, Kim YG (1991) J Chem Soc Chem Commun 849
20. Chung JS, Yun HG, Koh DJ, Kim YG (1993) J Mol Catal 79:199
21. Homeyer ST, Sachtler WMH (1989) J Catal 118:266
22. Feeley JS, Sachtler WMH (1991) J Catal 131:573
23. Zhang Z, Zhang YD, Hines WA, Budnick JI, Sachtler WMH (1992) J Am Chem Soc 114:4834
24. Ryoo R, Cho SJ, Pak CH, Kim JG, Ihm SK, Lee JY (1992) J Am Chem Soc 114:76
25. de Graaf J, van Dillen AJ, de Jong KP, Koningsberger DC (2001) J Catal 203:307
26. Guczi L, Beck A, Horva′th A, Horva′th D (2002) Top Catal 19:157

27. Sun T, Seff K (1994) Chem Rev 94:857
28. Seidel A, Loos J, Boddenverg B (1999) J Mater Chem 9:2495
29. Farzaneh F, Oskooie MK, Nejad M (1989) J Sci Ir 1:23
30. Murat M, Amokrane A, Bastide JP, Montanaro L (1992) Clay Mine 27:119
31. Chandrasekhar S, Pramada PN (1999) J Por Mater 6:283
32. Chang HL, Shih WH (2000) Ind Eng Chem Res 39:4185
33. Rayalu S, Meshram SU, Hasan MZ (2000) J Hazard Mater 77:123
34. Querol X, Moreno N, Umaña JC, Alastuey A, Hernández E, López-Soler A, Plana F (2002) Int J Coal Geo 50:413
35. Srinivasan A, Grutzeck MW (1999) Environ Sci Technol 33:1464
36. Ojha K, Pradhan NC, Samanta AN (2004) Bull Mater Sci 27:555
37. Fotovat F, Kazemian H, Kazemeini M (2008) Mater Res Bull (in press)
38. Ginter M, Bell AT, Radke CJ (1992) In synthesis of microporous materials, vol 1. Van Nosstrand Reinhord, New York
39. Tang Q, Wang Y, Zhang Q, Wan H (2003) Catal Commun 4:253
40. Tang Q, Zhang Q, Wang P, Wang Y, Wan H (2004) Chem Mater 16:1967
41. Ravishankar R, Li MM, Borgna A (2005) Catal Today 106:149
42. Sun S, Tsubaki N, Fujimoto K (2000) Appl Catal A 202:121
43. Boot LA, Kerkhoffs MHJV, van Dillen AJ, Geus JW, van Buren FR, van der Linden BTh (1996) Appl Catal A 137:69
44. Panpranot J, Goodwing JG Jr, Sayari A (2002) Catal Today 77:269
45. Jacobs G, Das TK, Zhang Y, Li J, Racoillet G, Davis BH (2002) Appl Catal A 233:263
46. Iglesia E, Soled SL, Fiato RA (1992) J Catal 137:212
47. Reuel RC, Bartholomew CH (1984) J Catal 85:78
48. Iglesia E (1997) Appl Catal A 161:59